Journal Pre-proofs

Sponge-like carbon monoliths: porosity control of 3D-printed carbon supports and its influence on the catalytic performance

Cristian Chaparro-Garnica, Esther Bailón-García, Arantxa Davó-Quiñonero, Dolores Lozano-Castelló, Agustín Bueno-López

PII: S1385-8947(21)05791-0
DOI: https://doi.org/10.1016/j.cej.2021.134218
Reference: CEJ 134218

To appear in: *Chemical Engineering Journal*

Received Date: 11 October 2021
Revised Date: 29 November 2021
Accepted Date: 14 December 2021

Please cite this article as: C. Chaparro-Garnica, E. Bailón-García, A. Davó-Quiñonero, D. Lozano-Castelló, A. Bueno-López, Sponge-like carbon monoliths: porosity control of 3D-printed carbon supports and its influence on the catalytic performance, *Chemical Engineering Journal* (2021), doi: https://doi.org/10.1016/j.cej.2021.134218

Sponge-like carbon monoliths: porosity control of 3D-printed carbon supports and its influence on the catalytic performance.

Cristian Chaparro-Garnica, Esther Bailón-García, Arantxa Davó-Quiñonero, Dolores Lozano-Castelló, Agustín Bueno-López.*

[a]Departamento de Química Inorgánica, Universidad de Alicante, Carretera de San Vicente del Raspeig s/n, E03080, Alicante (España).

Keywords: 3D printing; CO-PrOx; monolith; carbon gel; porosity control.

Corresponding author: E. Bailón-García

E-mail: estherbg@ugr.es

Abstract

Sponge-like carbon monoliths with tailored channel architecture and porosity were prepared by combining sol-gel polymerization and 3D printing technology. The pore size distribution (PSD) and macropore volume were controlled by varying the water concentration used in the synthesis. The size and interconnection degree of primary particles, and consequently the pore width and macropores volume, increases by increasing the water concentration. However, a more heterogeneous PSD was detected at high water concentration, due to the better-defined spheres-like morphology of primary particles which leaves voids and corners between fused spheres together with bigger macropores leaves by the coral-like structure. The role of this porosity control on the CuO/CeO_2 catalytic performance was pointed out in the CO-PrOx reaction. The CuO/CeO_2 dispersion and distribution along the carbon network increases by increasing the water concentration, i.e. the pore width and macropore volume, enhancing the catalytic activity. However, this improvement is not observed at high water concentration in which preferential flow pathways are created favored by the heterogeneous PSD. This manifest that the porosity control plays an important role in the catalytic performance of monolithic catalysts and thus, the monolithic support must be specifically designed to optimize the catalytic performance of active phases for each application.

1. Introduction

Cellular monoliths are preferred over conventional fixed bed reactors in the industry for several reasons, like their low pressure drop, high mechanical resistance, better mass and heat transfer, reduction of incrustations and obstructions and easy handling for cleaning and maintenance [1,2]. Monoliths are commonly ceramic or metallic, each one with respective advantages and disadvantages [1,3]. Ceramic monoliths present higher thermal stability and better porosity and, thus, better adherence of the active phases coating, whereas metallic monoliths offer better heat transfer, pressure drop, mechanical stability, wall thickness and overall volume [4]. Ceramic monoliths are often preferred for catalytic applications due to the difficulty of catalyst adherence on the metallic ones.

Cordierite is the most extended material to prepare honeycomb ceramic monoliths due to its mechanical strength, negligible thermal expansion coefficient and favorable adherence properties [5,6]. However, the specific surface of cordierite monoliths is very low (ca. 2 m^2g^{-1}) to be properly used as adsorbent or catalytic support [4,7]. Thus, a coating of porous materials such as alumina, silica, oxides mixtures or carbon materials must be deposited on the cordierite monoliths to increase the specific surface [8]. Carbon materials are excellent candidates for that purpose due to their high surface area and pore volume, their chemical stability and their tailored textural and chemical properties [9–11]. Typical methods for monoliths coating are wash-coating and dip-coating with slurries containing high surface area powders. However, the surface area per total weight (or volume) could not be enough for several applications [12]. Thus, several attempts have been done to obtain integral carbon honeycomb monoliths. These integral honeycomb monoliths are mainly manufactured by extrusion of a paste composed by the carbon material or precursor, binders and organic or inorganic fillers, followed by a carbonization process. However, a strong shrink is obtained after the carbonization and the carbon porosity is

affected by the use of binders [13]. Therefore, the versatility of the porosity control of carbon materials is restricted by the imposed synthesis conditions. Thus, the search of new synthesis methodologies to obtain integral and purely carbon cellular monoliths with controlled porosity is a hot issue.

On the other hand, the technology available to obtain ceramic or even carbon monoliths mainly consist of extrusion technics. Thus, the morphology of the monoliths is limited to channeled designs consisting in straight channels which impose a laminar fluid flow through them. This imposed laminar flow creates radial mass and heat transfer limitations which avoid a proper performance of active phases. Therefore, the development of new technologies that allow obtaining more sophisticated monolith geometries which improve the fluid hydrodynamics and catalytic performance of usually expensive active phases could make a difference in the catalyst design at an industrial scale.

With both objectives in mind, obtaining integral and pure carbon monoliths with controlled textural properties and specifically 3D-designed geometry is the goal of this work. Taking into account that integral carbon pellets can be directly obtained without the addition of any binder or filler by the sol-gel polymerization and carbonization of organic monomers, carbon gels are presented as optimum candidates to obtain 3D controlled carbon monoliths with specific textural and chemical properties. These carbon gels are well-known by the nanometric control of their texture and chemical properties, high purity, chemical and thermal stability and versatility [14]. Carbon gels are formed by primary particles interconnected each other creating a well-defined, designed and controlled micro, meso and macroporous structure [15]. Additionally, their format can be controlled depending on the mold used in their synthesis. They can be also doped during synthesis with catalytically active phases and their surface chemistry is fully known and adjustable, giving rise to a wide range of materials with unique properties [16].

In a previous work [17], we have developed a new and advanced strategy to synthesize integral and purely carbon monoliths with controlled channels morphology by combining the versatility of the 3D-printing technology and the sol-gel polymerization. Two different channels architectures were designed and printed; a conventional honeycomb design composed by straight channels and an advanced tortuous design with channels that split and join successively along the monolith length to create a tortuous path, and the effect of the different channel morphology on the catalytic performance of CuO/CeO_2 active phase analysed in the CO preferential oxidation (CO-PrOx). Results showed that the existence of more tortuous channels in the monolith improve the availability of active sites to carry out the chemical reaction improving the catalytic performance and thus, demonstrates the potential of the 3D printing to improve the catalytic supports currently available. However, the porosity control can also play an important role in the improvement of the active phase dispersion and gas diffusion. Thus, taking advantage of the versatility of the sol-gel process, in this work, pure and integral carbon monoliths with specifically and rigorously designed geometry and porous texture are obtained and tested in the preferential oxidation of carbon monoxide (CO-PrOx reaction). This reaction is very important in the purification of hydrogen feed of PEM fuel cells since the H_2 synthesis is fossil fuel dependent, being mainly performed by steam reforming of short hydrocarbons [18]. Hydrogen generation via steam reforming leads to a H_2 feed with a variable CO content (10-12% vol.), that after a Water-Gas Shift (WGS) is reduced to 0.5-2%. However, this CO content in the H_2 stream is still too high to be directly fed in the PEM fuel cell, according to the well-known stringent ppmv CO-tolerance of Pt-based anodes and consequently, other purification processes are required to ensure the CO ppmv concentration level and to ensure the proper operation of Pt-based fuel cells anodes [19]. Among them, the CO-PRO) reaction has been claimed as the most promising approach.

This reaction has been widely studied and different active phase proposed such as noble metal-based catalysts (Pt, Pd, Rh, Ir, Ru dispersed into different metal oxide supports, such as Al_2O_3, SiO_2, zeolites, CeO_2-based supports) [20,21], Nano-gold catalysts (Au nanoparticles dispersed on TiO_2, Fe_2O_3, Al_2O_3, ZrO_2, CeO_2-based supports) [22–24] and mixed non-noble metal oxides (transition metal oxides, such as Co_3O_4 or CuO in combination with other major compounds forming binary mixtures in multiple configurations) [25,26]. Among them, CuO/CeO_2 catalysts present excellent activity and selectivity to CO oxidation in the low temperature range, acceptable CO_2 and H_2O compatibility, large stability and moderate price compared to noble metal-based catalysts and gold-supported materials [27,28]. Thus, CuO/CeO_2 was selected as the active phase to deposit on the prepared carbon monoliths.

2. Experimental Section

2.1. Catalyst Preparation

Active Phase Synthesis

CeO_2 was prepared by calcination of cerium nitrate hexahydrate ($Ce(NO_3)_3 \cdot 6H_2O$, 99.5% from Alfa Aesar) in a muffle at 500 ºC for 4 h. CuO/CeO_2 active phase was prepared with 5 wt.% Cu loading. For that, the appropriate amount of $Cu(NO_3)_2 \cdot 2.5H_2O$ (≥98% from Sigma-Aldrich) was dissolved in the minimum amount of water, according to the salt solubility, and added dropwise on the CeO_2 support. Then, the catalyst was flash dried in air in a preheated muffle at 200 °C, and finally, was treated at 400 ºC for 2h at a heating rate of 2 °C/min to decompose the CuO precursor salt and to obtain the final CuO/CeO_2 active phase.

3D-printed Monolithic Supports

The carbon monoliths were synthesized by polymerization of a mixture of resorcinol (R), formaldehyde (F) and water (W) following a modified Pekalas's method [29]. The R/F molar ratio was fixed in 1/2 whereas the R/W molar ratio was 1/13, 1/15 or 1/17 in order to control the porosity of the carbon gels. The reagent mixture was cast into a glass mold with the desired monolith diameter and a 3D-printed polymeric template, which acts as a negative of the desired channels architecture, was introduced in this mold in order to control the channel morphology. Several polymers were tested and Co-polyester (CPE+) was selected as polymer to print the template due to its high chemical stability. The templates were printed using an Ultimaker 2+ 3D printer. The polymeric template was printed with a tortuous design described in more detail afterwards. The polymerization and cure process involves 1 day at room temperature, 1 day at 50 ºC and 5 days at 80 ºC. After curing, the organic gel was unmolded and cut to the desired length. The water filling the porosity was exchanged by acetone during 3 days, exchanging acetone twice daily, to favor the drying process. The drying process involves 3 days at room temperature and 1 day at 50 ºC. Carbon monoliths were obtained from these green monoliths by carbonization in N_2 flow at 900 ºC with a soak time of 2 h and a heating rate of 1 ºC/min. The green monolith dimensions shrink by 20 % after carbonization. The dimensions of the final carbon monoliths are 1 cm diameter and 1.7 cm length. A scheme of the carbon monolith synthesis is depicted in **Figure 1**.

A honeycomb cordierite monolith of cell density of 200 cpi (named as HCM) and the same dimensions that the prepared carbon monoliths was purchased from Corning Inc. and used as reference.

Active-phase loading into the monoliths

CuO/CeO_2 active phase was dispersed in ethanol (15 wt. %), stirred for 1 h and finally loaded on the monolith by dip-coating under stirring (**Figure 1**). The impregnated monoliths were dried rotating horizontally for 24 h at room temperature, and then, treated at 250 ºC in static air for 24 h at a heating rate of 4 ºC/min. Finally, the excess of active phase that could obstruct the channels and that is not adhered to the support was eliminated by means of compressed air. One impregnation was required for 1/17 and 1/15 carbon monoliths, two for 1/13 and six for the cordierite monolith to load the same amount of active phase (110 ± 5 mg).

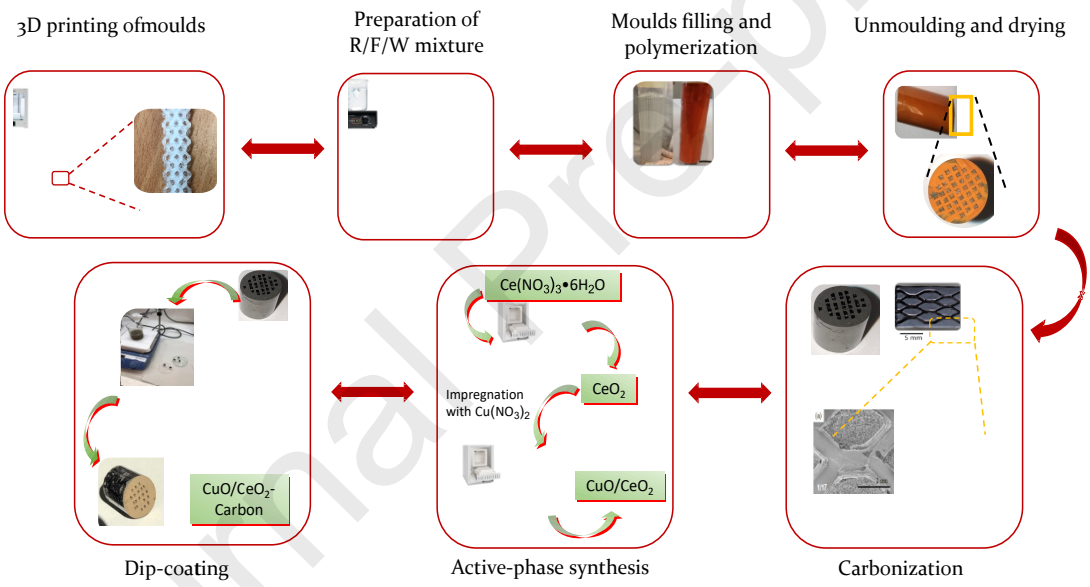

Figure 1. Scheme of the synthesis of CuO/CeO_2-carbon monoliths.

2.2. Catalyst characterization

The amount of CuO/CeO_2 loaded into the carbon monoliths was determined from the weight increase after the dip coating process of the dried monoliths, and was corroborated by burning the supported catalysts at 700 ºC for 2 h.

The thermal stability of the carbon monoliths, both fresh and loaded with CuO/CeO_2, was determined by thermogravimetric analysis using an SDT 2960 DSC-TGA equipment. In a typical experiment, temperature was raised at 10 ºC/min up to 900 ºC under air flow.

Textural properties of carbon monoliths were studied by gas adsorption measurements (N_2 at -196 ºC) and Hg-porosimetry using an Autosorb-6B equipment and a Poremaster 60 GT, respectively from Quantachrome. Before the analysis, carbon samples were degassed at 110 ºC for 8 h.

The CuO/CeO_2 distribution on the carbon monolith surface was examined by scanning electron microscopy (SEM) using a S-3000N microscope from HITACHI equipped with an XFlash 3001 X-ray detector from Bruker for microanalysis (EDS) and chemical mapping.

2.3. Catalytic Tests

The catalytic performance of supported catalysts was tested in the preferential oxidation of CO (CO-PrOx). In a typical reactivity test, the monolithic catalyst was perfectly fitted in a stainless-steel cylindrical reactor using Teflon tape. The reaction gas mixture, consisting of 2% CO, 2% O_2, and 30% H_2 balanced in He, was fed to the reactor for 30 min at room temperature and then, the temperature was increased to 250 ºC at a heating rate of 2 °C/min. Experiments were performed with total flows of 60, 90, 120 and 150 mL/min. The outflow gases were analyzed using a gas chromatograph (Agilent Technologies 6890N) equipped with two columns: Porapak Q 80/100 for CO_2 and H_2O separation and Molecular Sieve 13X for O_2 and CO separation. After the reaction, the gas mixture was replaced by 5% O_2 in He and the temperature was maintained at 250 ºC for 15 min. Finally, the furnace was switched off and the reactor was cooled down in O_2/He without control of the cooling rate. Several reaction cycles were performed to corroborate

the catalysts stability. The CO conversion and selectivity to CO oxidation were calculated by the following equations:

$$C_{CO} = \text{CO conversion } (\%) = \frac{[CO]in - [CO]out}{[CO]in} \cdot 100 \quad (1)$$

$$S_{CO} = \text{CO selectivity } (\%) = \frac{[CO]in - [CO]out}{[O2]in - [O2]out} \cdot \frac{1}{2} \cdot 100 \quad (2)$$

3. Results and discussion

3.1. Characterization of CuO/CeO_2-carbon monolith catalysts

Carbon monoliths were prepared by sol-gel polymerization of resorcinol and formaldehyde (RF) following a modified Pekala's method [29], and monoliths with controlled channel architectures were obtained by introducing 3D-printed polymeric templates (**Figure 2a**) inside glass tubes before the RF polymerization took place (**Figure 2b**). This aqueous mixture perfectly fills up all the free space left by the template without generation of air bubbles even at the interfacial region, denoting good wettability of the template with the RF solution. Robust and resistant carbon monoliths were obtained after carbonization (**Figure 2c**) without adding binders or fillers that can affect the porosity control of the carbon monoliths. The polymeric template was removed during the carbonization process and a perfect negative of the channel architecture of the polymeric template was reproduced without any crack in the carbon walls (**Figure 2d**). The hardiness and resistance of the monolith is also evidenced in **Figure 2d** by the fact that the monolith can be cleanly cut without breaking or crumbling. Thus, the complete filling and good wettability of the template allows obtaining advanced and complex designs using this combined sol-gel and 3D-printing methodology. Moreover, by this combined method not only the channel architecture can be designed and controlled but also the versatility of the sol-gel process allows a rigorous control and design of the carbon porosity by adjusting the different variables involved during their synthesis.

The textural properties of 3D-designed carbon monoliths were controlled by varying the Resorcinol (R)/Water (W) molar ratio. This R/W ratio was varied from 1/13 to 1/17 and different textural morphologies were obtained, as observed by FESEM (**Figure 3**). A smooth surface is observed at the channels interface (**Figure 3a**), which looks similar for all monoliths regardless the R/W ratio used. This smooth surface can be ascribed to the presence of carbon deposit left by the polymeric template upon pyrolization or to a different polymerization reaction in the solution-polymer interface due to the interaction of the RF mixture and the polymeric template, as occurs at the solution-glass interface that looks very sparkly (see **Figure 3c**).

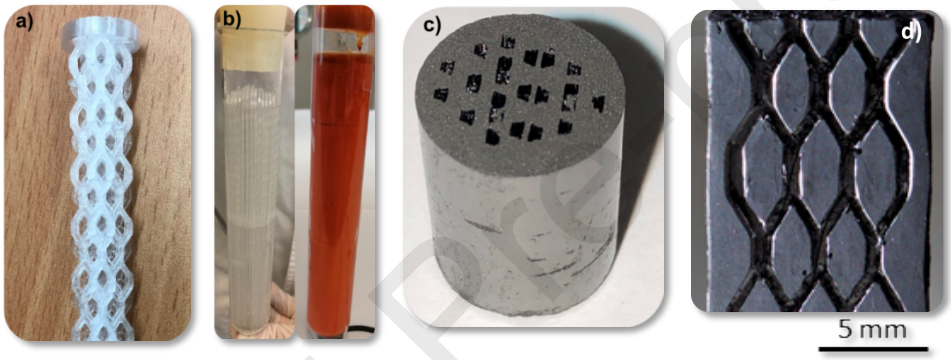

Figure 2. Images of the 3D printed template (a), 3D template and RF formaldehyde mixture into glass tube before and after polymerization (b) and top view and (c) cross section (d) of the obtained carbon monolith

A very rough and macroporous surface is identified in the carbon bulk, with a sponge-like carbon structure for all R/W molar ratios. It is known that the R/W molar ratio influences the texture of carbon gels [30]. The polycondensation of RF produces clusters of macromolecules that react with each other and grow into colloidal particles [31]. Finally, a cross-linked network of interconnected colloidal particles is obtained. Thus, by varying the size and interconnection degree of these primary particles, the pore size distribution can be adjusted from micro, meso to macropores. The size and the number of these colloidal particles as well as their aggregations to three dimensional networks are strongly affected by the reagent concentration [32]. The growth rate of these individual

colloidal particles becomes larger by decreasing R/W [31] and thus, their size increases, the interconnection degree between them decreases and, consequently, the mean width of pores increases. This was clearly observed by FESEM (**Figure 3**). At high R/W ratio (1/13; **Figure 3b**), small and high-interconnected primary particles are obtained leaving the smallest pore size width of the series (1000 nm) but the most homogeneous macroporous structure. Decreasing the R/W ratio (i.e. 1/15 or 1/17), the size of these primary particles increases, and their interconnection degree decreases leaving larger pores (>10000 nm). It is also important to highligh that the morphology drastically changed decreasing the R/W ratio from 1/15 to 1/17. At R/W lower than 1/15, the interconexion degree is so high that primary particles are not observed, while spherical particles are clearly identified at R/W=1/17. Moreover, a more heterogeneous macroporous structure is observed, mainly at R/W=17. In such case, small interparticle voids and corners are detected between primary spheres as well as big voids raging from 10 to 40 μm are also detected.

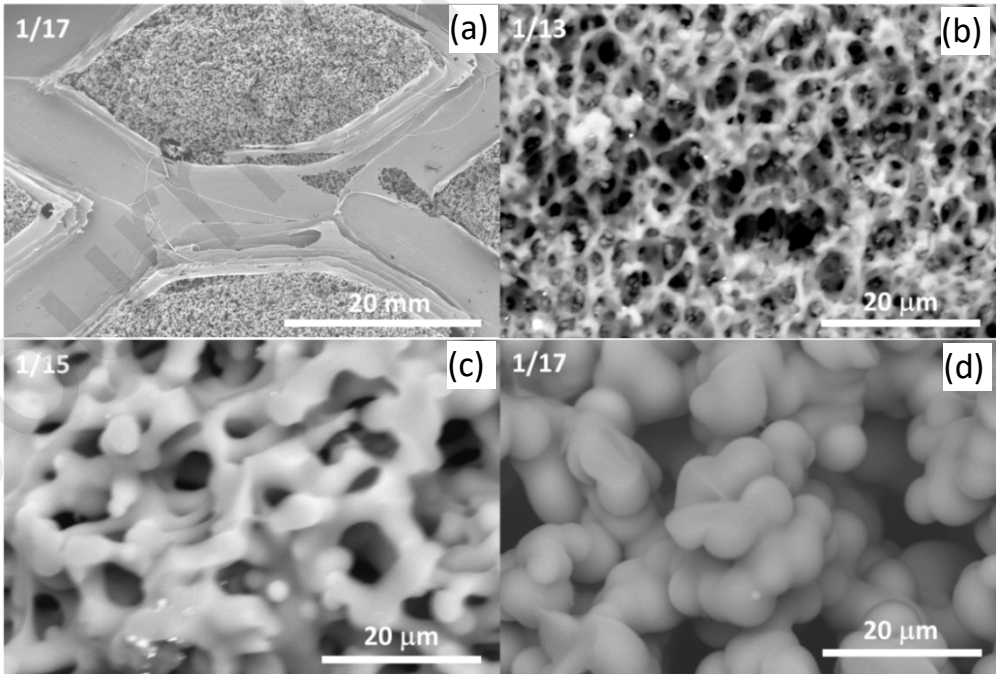

Figure 3. SEM images of the carbon monoliths. Detail of the channels for the monolith prepared with resorcinol/water (R/W) molar ratio = 1/17 (a) and pictures of the carbon bulk for R/W (b) 1/13, (c) 1/15 and (d) 1/17.

This different macroporous texture was confirmed by Hg porosimetry and N_2-adsorption (**Figure 4**). Type II N_2-adsoption isotherms (**Figure 4a**) were obtained for all R/W molar ratios, characteristics of non-porous or macroporous adsorbents. Thus, to characterize this macroporosity, Hg-porosimetry was performed (**Figure 4b**). Note that, as was previously observed by FESEM, the pore width and macropores volume increases by decreasing the R/W ratio from 1/13 (V_{macro}=0.82 cm^3g^{-1}) to 1/15 (V_{macro}=1.06 cm^3g^{-1}) and 1/17 (V_{macro}=1.52 cm^3g^{-1}). At low water concentration (R/W=1/13), a well-defined peak is obtained centred at a mean pore diameter of 1000 nm, whereas increasing the water amount (W=15 and 17), more heterogeneous pore size distributions are obtained with a mean pore diameter centred at 14000 nm and 16000 nm, respectively. At R/W=1/17, smaller (3000 nm) and bigger (40000 nm) pores are also detected, corroborating the more heterogeneous macroporous structure of this sample observed by FESEM. Concluding, the porosity of the carbon gel monoliths can be set by modifying the sol-gel polymerization conditions depending on the application necessities.

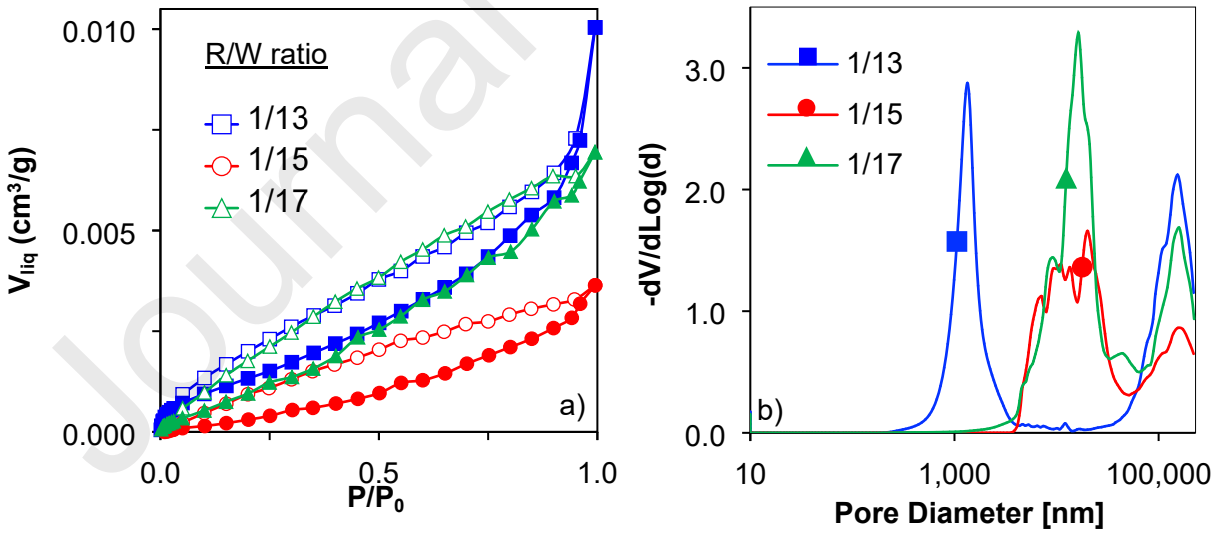

Figure 4. Characterization of textural properties of carbon monoliths prepared with different resorcinol/water (R/W) molar ratio. a) N_2-adsorption isotherms and b) pore size distribution obtained by Hg-porosimetry.

The large pores obtained can be very appropriate for the dispersion of the CuO/CeO_2 active phase particles. This CuO/CeO_2 active phase is well-known and it was already characterized in previous works [33,34], so, data are included in supporting information. The amount of active phase anchored in each of the monoliths (1/13, 1/15 and 1/17) was very similar for all of them (110 ± 5 mg). To determine the amount of CuO/CeO_2 loaded on each carbon monolith, the weight was monitored before and after the dip coating process. Furthermore, these amounts were also corroborated by burning the supported catalysts (sacrificial samples with the same preparation conditions) at 700 ºC for 2 h. The dispersion of the CuO/CeO_2 active phase on the carbon monoliths and the effect of the porous texture on this dispersion was pointed out by FESEM (**Figure 5** and **Figure S4**). Overall, the CuO/CeO_2 dispersion increases by decreasing the R/W molar ratio and thus, increasing the macropores volume and pore width (**Figure 5, centre**). A channel split is observed in **Figure 5 left** for all R/W ratios. Note that most of the active phase is mainly located on the channel surface for a R/W molar ratio of 1/13, blocking in part the entrance of some porosity. However, by decreasing the R/W molar ratio, not only the dispersion of the active phase on the channel surface is improved, but also distribution inside the carbon network (**Figure 5 left and right**) due to the pore width widening and so, the improved diffusion of the active phase aqueous suspension inside the carbon network. Note also that, for the R/W=1/17 sample, a high quantity of active phase is well-dispersed in the smaller voids between the spherical particles.

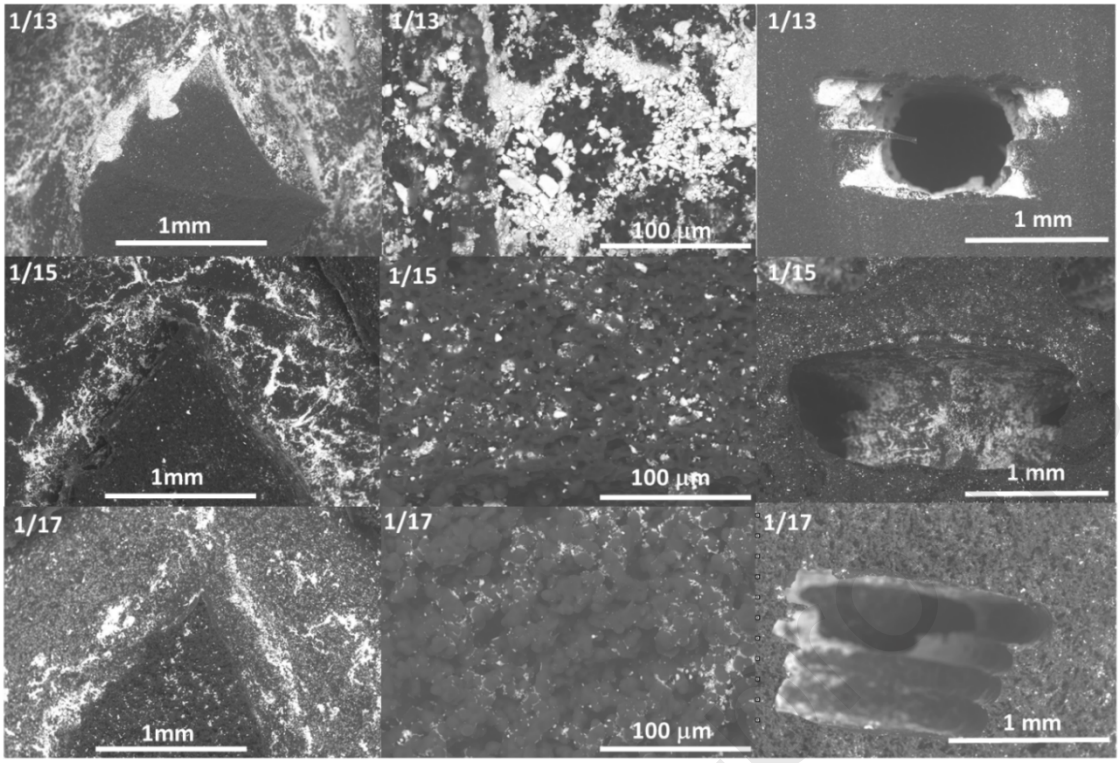

Figure 5. Distribution of CuO/CeO_2 active phase (white) on the surface of carbon (grey) monoliths prepared with different R/W molar ratio. Left: Channel Branch, centre: Channel wall and Right: channel entrance (transversal section).

This different active phase dispersion as well as its distribution along the carbon monolith network can affect the active phase catalytic behaviour. CuO/CeO_2 is a well-known oxidation catalyst and, taking into account the carbon nature of the monoliths, the presence of CuO/CeO_2 and its dispersion and distribution along the monolith can affect their stability in oxidizing atmospheres. To analyse the stability of the carbon monoliths-supported CuO/CeO_2 under oxidizing conditions, thermogravimetric analysis in air flow were performed to monoliths with and without active phase, and results are depicted in **Figure 6**. The active phase-free monoliths start to get burnt at around 550 ºC, and this onset temperature is not significantly affected by the R/W ratio used in the monolith synthesis. The addition of CuO/CeO_2 favors the carbon combustion (the burn off onset is ~500 ºC), and the combustion rate (slope of the curve) depends on the R/W ratio. Since the reactivity of carbon is similar in the absence of active phase, different combustion

rates could be attributed to the distribution of CuO/CeO_2 into the carbon network. One hypothesis to explain differences could be that, at high R/W ratio (1/13), most active phase is located on the outer surface of the channels, blocking part of the carbon porosity and avoiding air diffusion into the carbon network, therefore obtaining the slowest combustion rate (lowest slope in the thermogram). Decreasing the R/W ratio, the active phase dispersion and distribution into the carbon network is improved, favoring the active phase-carbon contact, and promoting faster carbon combustion. Another hypothesis could be that carbon combustion starts with CuO/CeO_2 oxygen, and once the carbon surface is oxidized by active phase oxygen, gas phase oxygen is able to continue the combustion. If this is the case, the better the carbon-active phase contact, the faster the combustion, and the improved dispersion of CuO/CeO_2 by decreasing the R/W ratio would explain the faster combustion rate.

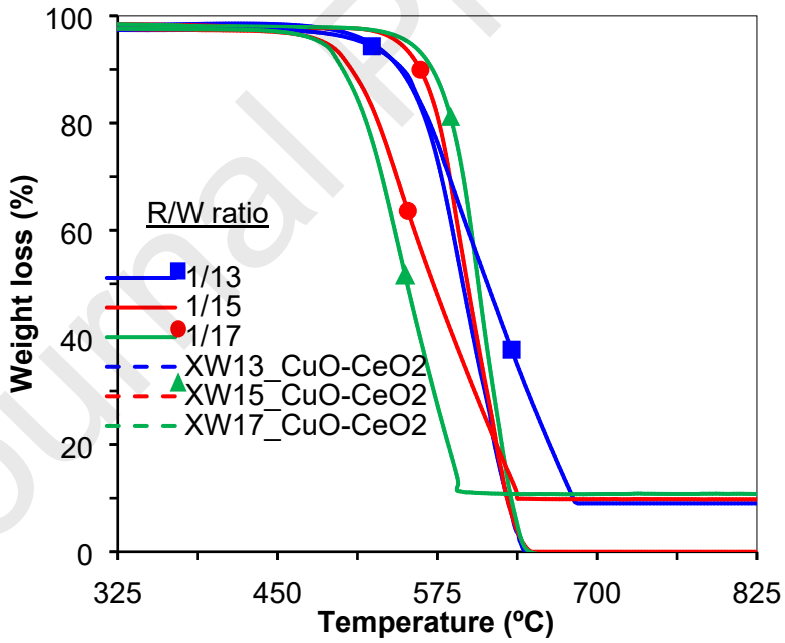

Figure 6. Thermogravimetric analysis in air of pure (continuous line) and CuO/CeO_2-containing (dashed line) carbon monoliths prepared with different resorcinol/water (R/W) molar ratio.

Nevertheless, the thermal stability of all supported catalysts in oxidizing conditions (≥ 500 ºC) is high enough to allow the use of these carbon-based monolithic catalysts in a wide range of reactions.

3.2. Catalytic tests: CO oxidation in CO-PrOx conditions

The catalytic performance of the carbon monoliths-supported CuO/CeO_2 was studied in the oxidation of CO in CO-PrOx conditions (2% CO, 2% O_2, and 30% H_2 in He balance) and results are collected in **Figure 7**. As it was already mentioned, a similar amount of active phase was loaded in all carbon monoliths (115 ± 10 mg). CO conversion and selectivity to the CO oxidation for catalysts supported on the monoliths prepared with the different R/W molar ratios are depicted in **Figure 7** for flow rate of 60 and 120 mL/min. Note that, as expected, the CuO/CeO_2 active phase is very active and selective for the CO preferential oxidation, but its catalytic performance is clearly influenced by the carbon monolith synthesis conditions (**Figure 7a**). An increase in the flow from 60 to 120 cm^3/min slightly decreases the conversion for monolith prepared with R/W=1/13 and 1/15. However, this increase in the flow highly affects the conversion in the case of R/W=1/17 sample. At both flow rates, the lowest conversion was obtained using the carbon monolithic support prepared with a R/W ratio of 1/13. The conversion highly increased by increasing the R/W ratio from 1/13 to 1/15. This can be explained based on the porous texture and thus, the CuO/CeO_2 dispersion obtained. As it was previously pointed out, the porous width and macropores volume increases by decreasing the R/W ratio and thus, the active phase dispersion is improved. The improved dispersion of the active phase increases the available active sites for CO oxidation and enhances the catalytic performance. By decreasing the R/W ratio from 1/15 to 1/17, an increase in conversion could be also expected since better active phase dispersion is observed. However, this increase is not observed but a different behaviour is obtained depending

on the flow rate. The effect of the increase of the flow rate from 60 to 120 cm^3/min on the conversion of R/W=1/13 and 1/15 samples is almost negligible whereas this effect is important for the R/W=1/17 sample (**Figure 7a**). A similar activity to that of R/W=1/15 sample is obtained at low flow rate (60 cm^3/min), whereas, at high flow rates (120 cm^3/min) the conversion and reaction rate highly decrease. This different behaviour of 1/17 sample can be explained based on the different pore size distribution of carbon monolith and the active phase distribution along its porosity, which play an important role on the gas diffusion through the carbon network and thus, on the active phase activity. Therefore, to analyse the effect of mass diffusion on the reaction rate, several gas flows rates ranging from 60 to 120 mL/min were used and CO conversion rate normalized by weight of CuO/CeO_2 at 70 ºC is shown in **Figure 8** as function of the flow rate. It is observed that the normalised reaction rate obtained with 1/13 and 1/15 samples increases by increasing the flow rate, which indicates that the active phase in these samples work under diffusional control in all the flow rate range tested. However, the normalised reaction rate obtained with the sample 1/17 is only slightly affected by the gas flow, indicating that the active phase in this sample is working under near chemical control of the reaction rate. According to this observation, it can be concluded that the active phase dispersed on the 1/17 carbon monolith support is less efficient than the same active phase dispersed on the 1/15 support. The 1/17 monolith is able to reach the chemical control rate, that is, reaches the fastest CO oxidation rate possible, but this rate is slower to that achieved with 1/15, which reacts under diffusion control and still has room for the improvement at higher gas flows.

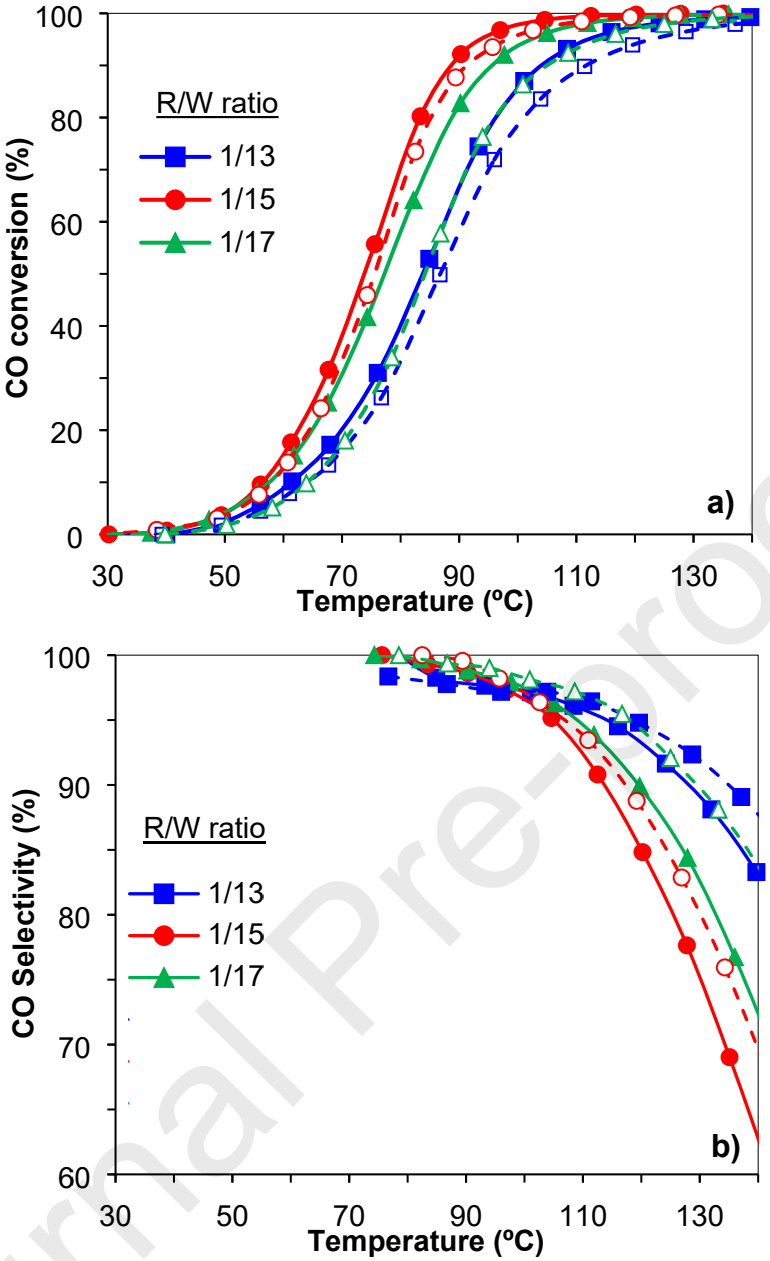

Figure 7. a) Conversion of CO (C_{CO}) and b) selectivity to CO (S_{CO}) of the CuO/CeO_2 active phase supported on carbon monoliths prepared with different R/W molar ratios. Gas flow of 60 cm^3/min (continuous line) and 120 cm^3/min (dashed line).

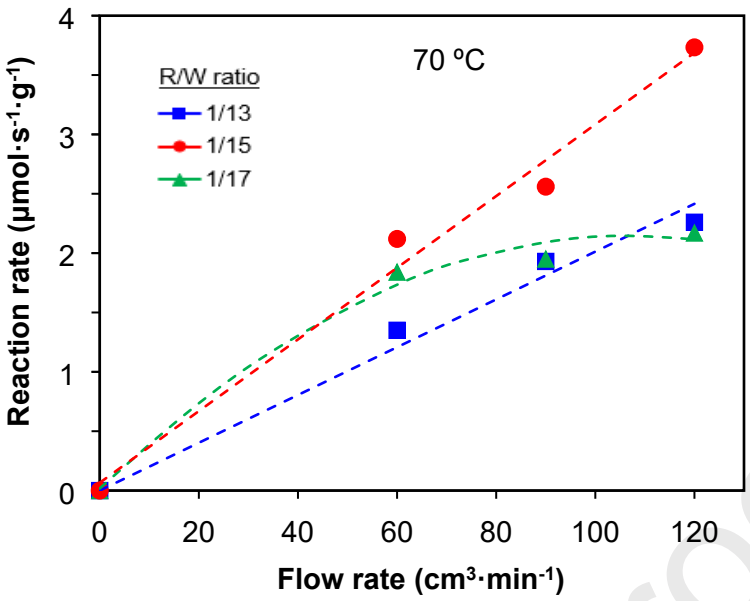

Figure 8. CO conversion rate normalized by weight of CuO/CeO_2 as a function of the flow rate for catalysts supported on carbon monoliths prepared with R/W=1/13, R/W=1/15 and 1/17.

In order to explain the different behaviour of the CuO/CeO_2 active phase on the different carbon monolith supports, two opposite effects must be considered that can be acting together: the dispersion of the active phase and its distribution along the carbon network and thus, its accessibility. The active phase dispersion increases by decreasing the R/W ratio enhancing the catalytic activity, however, the distribution of this active phase along the carbon network increases in that sense, which can be in detriment of the catalytic activity due to a hindered accessibility to the active phase. Thus, an optimum of these two factors can be obtained for a R/W ratio of 1/15. Nevertheless, the porosity obtained is too high (micrometer range) to completely hinder the gas accessibility inside such porosity. In a previous work [35], for 1/15 sample, it has been pointed out that at flows lower than 150 cm^3/min, gas mainly circulates thorough the carbon network and thus, active phase inside the carbon network is accessible to the gas flow and thus, active. Moreover, the tortuous pathway of the channels creates turbulence which also favours the diffusion

inside such porosity. Thus, the active phase inside the porosity is accessible and active. Consequently, an increase of dispersion, as it is observed decreasing the R/W ratio, should improve the catalytic activity. However, this could be observed if the flow diffusion through the carbon network was homogeneous, and no preferential pathways are produced. As it was pointed out in the characterization section, carbon network morphology is similar for 1/13 and 1/15, primary particles highly fused forming a cross-linked network of polymer chains which left a homogeneous pore size distribution and thus, can favours a homogeneous gas flow thorough the carbon network. Nevertheless, this morphology deeply changes decreasing the R/W to 1/17. Now, spherical-shaped fused primary particles are obtained, and thus, a more heterogeneous pore size distribution is obtained with pores ranging from small macropores (3000 nm) to big macropores (40000 nm). Thus, preferential pathways can be produced favoured by the heterogeneous pore size distribution of this sample and consequently, the CuO/CeO_2 active phase mainly localized in the small interparticle voids and corners detected between primary spheres are not accesible, decreasing the activity. By increasing the flow, the creation of this preferential pathways is favoured, and the activity decrease is more significant. Overall, a homogeneous pore size distribution with an optimum pore size to well disperse the active phase is optimized at a R/W ratio of 1/15 in such a way that a good active phase dispersion and an homogeneous gas diffusion through the carbon network are obtained which maximize the catalytic performance of the CuO/CeO_2 active phase in the CO-PrOx reaction.

An isothermal catalytic test was performed at 104 ºC for long time (10 h) using the carbon-based monolithic catalyst (R/W 1/15), in order to analyse the stability. Results in **Figure 9** show that both CO conversion (98%) and CO selectivity (99%) remain almost

constant or even increases during all the experiment time indicating that this catalyst is very stable for long reaction time.

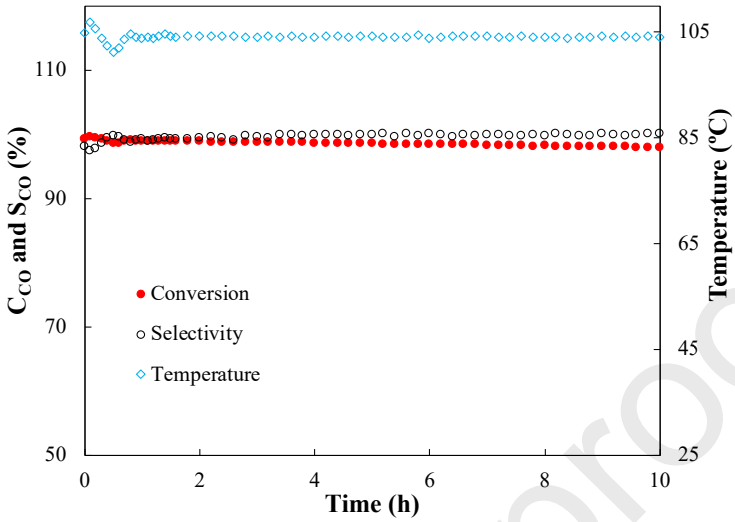

Figure 9. CO conversion (C_{CO}) and selectivity to CO oxidation (S_{CO}) (in the main axis) and temperature (in the secondary axis) for the CuO/CeO_2 supported on carbon monolith prepared with R/W=1/15. Reaction conditions: 2% O2, 2% CO, 30% H_2, and He balance. Total flow of 60 mL/min at constant temperature (104 ºC).

Finally, the activity of the CuO/CeO_2 supported on this new and advanced 3D printed sponge-like carbon monolith (1/15) was compared with the one supported on a conventional honeycomb cordierite monolith (HCM). CO conversion rate normalized by weight of CuO/CeO_2 is depicted in **Figure 10**. Note that despite the lower gas hourly space velocity (GHSV) of the cordierite monolith (6684 h^{-1}) regarding the carbon monolith (17910 h^{-1}), which favors the catalytic conversion due to the high residence time of gases [36,37], the CO conversion rate of the active phase supported on the carbon monolith is almost twice of the active phase supported on the honeycomb cordierite monolith. This means the carbon supports allows that the catalyst converts a high feed flow rate, and a low reactor volume could be used. This pointed out the benefits that this new 3D printed carbon monoliths could entail in the heterogeneous catalysis fields.

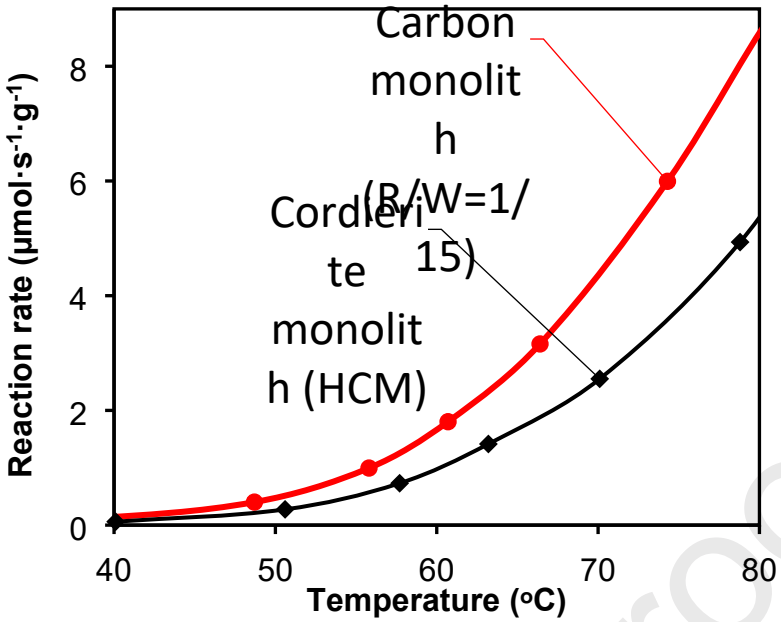

Figure 10. CO conversion rate normalized by weight of CuO/CeO_2 for catalysts supported on a 3D-printed carbon monolith prepared with R/W=1/15 and a conventional honeycomb cordierite monolith (HCM)

4. Conclusions

In this work, pure and integral carbon monoliths with specifically and rigorously designed geometry and porous texture were obtained by combining the sol-gel polymerization of resorcinol and formaldehyde and the 3D printing technology. These advanced monoliths have been used as catalytic support of the CuO/CeO_2 active phase and the catalytic performance studied in the preferential oxidation of CO (CO-PrOx). The role of the porosity control on the catalytic performance of this active phase was clearly pointed out by the modification of the textural properties, that is, porosity width of monolith carbon network by varying the resorcinol/water molar ratio used during the synthesis. Sponge-like structures were obtained by this synthesis method; however, the water concentration plays an important role in the porosity size distribution and macropores volume. Low water concentration produces carbon gels networks composed by high fused primary particles leaving smaller but more homogeneous pore size distribution (1000 nm).

However, primary particles size increases by increasing the water concentration, increasing the pore size and macropores volume. At high water concentration, clearly spherical primary particles were obtained but a more heterogeneous pore size distribution was detected due to small interparticle voids and corners between primary spheres joined to the more opened carbon gels network. This different pore size distribution and macropore volume affect the active phase distribution and, consequently the catalytic performance. The active phase dispersion increases by increasing the water concentration, and thus the pore volume and pore width. This improved dispersion enhanced the catalytic activity, however at high water concentration, this improvement is not observed. This less efficient catalytic performance of the active phase can be explained based on two opposite effects that can be acting together: the dispersion of the active phase and its distribution along the carbon network and thus, its accessibility. The heterogeneous pore size distribution of this sample can favours the creation of preferential pathways and consequently, the CuO/CeO_2 active phase that are localized in the small interparticle voids and corners detected between primary spheres are not accessible, and thus not active. Overall, a homogeneous pore size distribution with an optimum pore size to well disperse the active phase is optimized by controlling the water concentration in such a way that a good active phase dispersion and an homogeneous gas diffusion through the carbon network are obtained which maximize the catalytic performance of the CuO/CeO_2 active phase in the CO-PrOx reaction.

5. Acknowledgements

The authors thank the financial support of the Spanish Ministry of Economy and Competitiveness (Project CTQ2015-67597-C2-2-R), University of Alicante (Project GRE18-01A), Generalitat Valenciana (Project PROMETEO/2018/076, PhD grant

GRISOLIAP/2017/177 and contract APOSTD/2019/030) Junta de Andalucía (Project P18-RTJ-2974) and the UE (FEDER funding).

6. Data availability

The data that support the findings of this study are available from the corresponding author on request.

7. References

[1] S. Govender, H. Friedrich, Monoliths: A Review of the Basics, Preparation Methods and Their Relevance to Oxidation, Catalysts. 7 (2017) 62. https://doi.org/10.3390/catal7020062.

[2] B. Mitra, D. Kunzru, Washcoating of Different Zeolites on Cordierite Monoliths, J. Am. Ceram. Soc. 91 (2008) 64–70. https://doi.org/10.1111/j.1551-2916.2007.02032.x.

[3] X. Xioading, H. Vonk, A. Cybulski, J.A. Moulijn, Alumina washcoating and metal deposition of ceramic monoliths, Stud. Surf. Sci. Catal. 91 (1995) 1069–1078.

[4] V. Tomasic, F. Jovic, State-of-the-art in the monolithic catalysts / reactors ˇic, Appl. Catal. A Gen. 311 (2006) 112–121. https://doi.org/10.1016/j.apcata.2006.06.013.

[5] J.L. Williams, Monolith structures, materials, properties and uses, Catal. Today. 69 (2001) 3–9. https://doi.org/10.1016/S0920-5861(01)00348-0.

[6] M.C. Bacariza, A.N. Mendes, C. Ozhan, P. Da Costa, C. Henriques, Optimizing Washcoating Conditions for the Preparation of Zeolite- Based Cordierite Monoliths for NOx CH4 - SCR : A Required Step for Real Application, Ind. Eng. Chem. Res. 58 (2019) 11799–11810. https://doi.org/10.1021/acs.iecr.9b01216.

[7] E. Pérez-Mayoral, V. Calvino-Casilda, E. Soriano, Metal-supported carbon-based materials: Opportunities and challenges in the synthesis of valuable products, Catal. Sci. Technol. 6 (2016) 1265–1291. https://doi.org/10.1039/c5cy01437a.

[8] F. Scheffler, P. Claus, S. Schimpf, M. Lucas, M. Scheffler, Heterogeneously Catalyzed Processes with Porous Cellular Ceramic Monoliths, in: M. Scheffler, P. Colombo (Eds.), Cell. Ceram. Struct. Manuf. Appl., Wiley-VCH, 2005: pp. 454–483.

[9] M. Titirici, R.J. White, N. Brun, V.L. Budarin, D.S. Su, F. del Monte, J.H. Clark, M.J. MacLachlan, Sustainable Carbon Materials, Chem. Soc. Rev. 44 (2015) 250–290.

[10] L.R. Radovic, Physicochemical Properties of Carbon Materials: A Brief Overview, Carbon Mater. Catal. (2008) 1–44. https://doi.org/doi:10.1002/9780470403709.ch1.

[11] T.J. Bandosz, Surface Chemistry of Carbon Materials, Carbon Mater. Catal. (2008) 45–92. https://doi.org/doi:10.1002/9780470403709.ch2.

[12] T. Valdés-Solís, G. Marbán, A.B. Fuertes, Preparation of microporous carbon-ceramic cellular monoliths, Microporous Mesoporous Mater. 43 (2001) 113–126. https://doi.org/10.1016/S1387-1811(00)00354-1.

[13] D.P. Vargas, L. Giraldo, J.C. Moreno-Piraján, CO2 adsorption on activated carbon honeycomb-monoliths: A comparison of Langmuir and Tóth models, Int. J. Mol. Sci. 13 (2012) 8388–8397. https://doi.org/10.3390/ijms13078388.

[14] F. Li, L. Xie, G. Sun, Q. Kong, F. Su, Y. Cao, J. Wei, A. Ahmad, X. Guo, C.M. Chen, Resorcinol-formaldehyde based carbon aerogel: Preparation, structure and applications in energy storage devices, Microporous Mesoporous Mater. 279 (2019) 293–315. https://doi.org/10.1016/j.micromeso.2018.12.007.

[15] J. Lee, S. Park, Recent advances in preparations and applications of carbon aerogels: A review, Carbon N. Y. 163 (2020) 1–18. https://doi.org/10.1016/j.carbon.2020.02.073.

[16] C. Moreno-Castilla, F.J. Maldonado-Hódar, Carbon aerogels for catalysis applications: An overview, Carbon N. Y. 43 (2005) 455–465. https://doi.org/10.1016/j.carbon.2004.10.022.

[17] C.Y. Chaparro-Garnica, E. Bailón-García, D. Lozano-Castelló, A. Bueno-López, Design and fabrication of integral carbon monoliths combining 3D printing and

sol-gel polymerization: Effects of the channel morphology on the CO-PROX reaction, Catal. Sci. Technol. 11 (2021) 6490–6497. https://doi.org/10.1039/d1cy01104a.

[18] A. Davó-Quiñonero, I. Such-Basáñez, J. Juan-Juan, D. Lozano-Castelló, P. Stelmachowski, G. Grzybek, A. Kotarba, A. Bueno-López, New insights into the role of active copper species in CuO/Cryptomelane catalysts for the CO-PROX reaction, Appl. Catal. B Environ. 267 (2020) 118372. https://doi.org/10.1016/j.apcatb.2019.118372.

[19] A. Davó-Quiñonero, S. López-Rodríguez, E. Bailón-García, D. Lozano-Castelló, A. Bueno-López, Mineral manganese oxides as oxidation catalysts: Capabilities in the Co-Prox reaction, ACS Sustain. Chem. Eng. 9 (2021) 6329–6336. https://doi.org/10.1021/acssuschemeng.1c00343.

[20] M. Kipnis, E. Volnina, New approaches to preferential CO oxidation over noble metals, Appl. Catal. B Environ. 98 (2010) 193–203. https://doi.org/10.1016/j.apcatb.2010.05.029.

[21] F. Mariño, C. Descorme, D. Duprez, Noble metal catalysts for the preferential oxidation of carbon monoxide in the presence of hydrogen (PROX), Appl. Catal. B Environ. 54 (2004) 59–66. https://doi.org/10.1016/j.apcatb.2004.06.008.

[22] M. Kipnis, Gold in CO oxidation and PROX: The role of reaction exothermicity and nanometer-scale particle size, Appl. Catal. B Environ. 152–153 (2014) 38–45. https://doi.org/10.1016/j.apcatb.2014.01.030.

[23] C. Rossignol, S. Arrii, F. Morfin, L. Piccolo, V. Caps, J.L. Rousset, Selective oxidation of CO over model gold-based catalysts in the presence of H2, J. Catal. 230 (2005) 476–483. https://doi.org/10.1016/j.jcat.2005.01.011.

[24] P. Lakshmanan, J.E. Park, E.D. Park, Recent Advances in Preferential Oxidation of CO in H2 Over Gold Catalysts, Catal. Surv. from Asia. 18 (2014) 75–88. https://doi.org/10.1007/s10563-014-9167-x.

[25] D. Li, X. Liu, Q. Zhang, Y. Wang, H. Wan, Cobalt and copper composite oxides as efficient catalysts for preferential oxidation of CO in H2-Rich stream, Catal. Letters. 127 (2009) 377–385. https://doi.org/10.1007/s10562-008-9693-0.

[26] E.D. Park, D. Lee, H.C. Lee, Recent progress in selective CO removal in a H2-rich stream, Catal. Today. 139 (2009) 280–290. https://doi.org/10.1016/j.cattod.2008.06.027.

[27] A. Davó-Quiñonero, A. Davó-Quiñonero, A. Davó-Quiñonero, E. Bailón-García, S. López-Rodríguez, J. Juan-Juan, D. Lozano-Castelló, M. García-Melchor, F.C. Herrera, F.C. Herrera, E. Pellegrin, C. Escudero, A. Bueno-López, A. Bueno-López, Insights into the Oxygen Vacancy Filling Mechanism in CuO/CeO2 Catalysts: A Key Step Toward High Selectivity in Preferential CO Oxidation, ACS Catal. 10 (2020) 6532–6545. https://doi.org/10.1021/acscatal.0c00648.

[28] F. Mariño, G. Baronetti, M. Laborde, N. Bion, A. Le Valant, F. Epron, D. Duprez, Optimized CuO-CeO2 catalysts for COPROX reaction, Int. J. Hydrogen Energy. 33 (2008) 1345–1353. https://doi.org/10.1016/j.ijhydene.2007.12.014.

[29] R.W. Pekala, D.W. Schaefer, Structure of Organic Aerogels. 1. Morphology and Scaling, Macromolecules. 26 (1993) 5487–5493. https://doi.org/10.1021/ma00072a029.

[30] C. Macías, P. Lavela, G. Rasines, M.C. Zafra, J.L. Tirado, C.O. Ania, On the correlation between the porous structure and the electrochemical response of powdered and monolithic carbon aerogels as electrodes for capacitive deionization, J. Solid State Chem. 242 (2016) 21–28. https://doi.org/10.1016/j.jssc.2016.06.019.

[31] T. Yamamoto, T. Yoshida, T. Suzuki, S.R. Mukai, H. Tamon, Dynamic and static light scattering study on the sol-gel transition of resorcinol-formaldehyde aqueous solution, J. Colloid Interface Sci. 245 (2002) 391–396. https://doi.org/10.1006/jcis.2001.8006.

[32] A. Hajizadeh, A.R. Bahramian, A. Seifi, I. Naseri, Effect of initial sol concentration on the microstructure and morphology of carbon aerogels, J. Sol-Gel Sci. Technol. 73 (2015) 220–226. https://doi.org/10.1007/s10971-014-3520-4.

[33] A. Davó-Quiñonero, M. Navlani-García, D. Lozano-Castelló, A. Bueno-López, J.A. Anderson, Role of Hydroxyl Groups in the Preferential Oxidation of CO over Copper Oxide-Cerium Oxide Catalysts, ACS Catal. 6 (2016) 1723–1731.

https://doi.org/10.1021/acscatal.5b02741.

[34] C.Y. Chaparro-Garnica, A. Davó-Quiñonero, E. Bailón-García, D. Lozano-Castelló, A. Bueno-López, Design of Monolithic Supports by 3D Printing for Its Application in the Preferential Oxidation of CO (CO-PrOx), ACS Appl. Mater. Interfaces. (2019). https://doi.org/10.1021/acsami.9b12731.

[35] C.Y. Chaparro-Garnica, E. Bailón-García, D. Lozano-Castelló, A. Bueno-López, Design and fabrication of integral carbon monoliths combining 3D printing and sol–gel polymerization: effects of the channel morphology on the CO-PROX reaction, Catal. Sci. Technol. (2021). https://doi.org/10.1039/d1cy01104a.

[36] S. Ascaso, M.E. Gálvez, P. Da Costa, R. Moliner, M.J. Lázaro-Elorri, Influence of gas hourly space velocity on the activity of monolithic catalysts for the simultaneous removal of soot and NOx, Comptes Rendus Chim. 18 (2015) 1007–1012. https://doi.org/10.1016/j.crci.2015.03.017.

[37] J. Gorimbo, A. Muleja, X. Liu, D. Hildebrandt, Fischer – Tropsch synthesis : product distribution , operating conditions , iron catalyst deactivation and catalyst speciation, Int. J. Ind. Chem. 9 (2018) 317–333. https://doi.org/10.1007/s40090-018-0161-4.

- Carbon monoliths with tailored channel architecture and porosity were synthesized
- The PSD and macropore volume were controlled by varying the synthesis conditions
- Active-phase dispersion and gas diffusion through the carbon network were optimized
- The role that the monolith porosity plays in the catalytic performance was studied
- The potential of 3D printing to improve the catalytic supports is demonstrated